Experimental Study on Bubble Dynamics in Water Surrogate Loop for Molten Salt Thermal Convection Loop(MSTCL) Applications

Hyunjin Booa, Suhyun Kima, Tae Hee Kima, Hwa Pyoung Kimb, Woo Seok Choib, Jong Won Kang b, Byung Gi Park a,*

^aDepartment of Energy & Environmental Engineering, Soonchunhyang University, Asan, Chungcheongnam-do

^bCentury Co., Magok Jungangro 86, Gangseo-gu, Seoul,

Corresponding author: byunggi@sch.ac.kr

*Keywords: Molten Salt Reactor, MSTCL, Bubble dynamics, Rising velocity, Clift model

1. Introduction

Molten Salt Reactors (MSRs) are Generation IV nuclear systems that employ fluoride- or chloride-based molten salts as both fuel and coolant. The thermophysical properties of molten salts allow stable liquid-phase operation at high temperatures under atmospheric pressure, providing MSRs with advantages in thermal efficiency, safety, and economics over conventional light water reactors (LWRs)[1].

During MSR operation, gaseous fission products such as xenon (Xe) and krypton (Kr) are generated. These inert gases reduce the neutron economy of the core and can lead to power instabilities. To mitigate this effect, MSR designs inject inert carrier gases such as argon to form bubbles, which transport the fission products to the cover gas system for removal. The resulting two-phase flow directly influences heat transfer and fluid dynamics. Therefore, understanding bubble formation, behaviour, and terminal velocity in molten salts is essential for safe operation and optimisation of the gas removal system[2,3].

Experimental studies have been actively conducted to investigate bubble dynamics in natural-circulation molten salt loops[2,3]. However, most previous work has been performed under straight-pipe conditions. In contrast, research-scale thermal convection loops are typically constructed in a skewed parallelepiped configuration. When bubbles are introduced at the lower section of the loop, both buoyancy and bulk flow act simultaneously, limiting the applicability of results derived from straight-pipe experiments.

To address this limitation, a transparent acrylic loop using water as the working fluid was constructed, and argon gas was injected into its inclined section. Bubble shape and rising velocity were quantified through image analysis, and the measured values under circulating flow conditions were distinguished from the terminal velocities of freely rising bubbles in stagnant fluids. Water, with its well-characterized thermophysical properties, is suitable for deriving dimensionless numbers such as the Eötvös, Morton, and Reynolds numbers, enabling scaling of the present results to molten salt conditions by accounting for differences in viscosity, density, and surface tension. Recent studies have also proposed recalibrating empirical correlations such as the Clift model to reflect medium-specific properties, and the present work adopts this approach to

interpret water-based data, thereby establishing a basis for extension to molten salt loop conditions[3]. Accordingly, this experiment serves as a preliminary step toward building a database in water that supports the development of scaling and modeling approaches applicable to molten salt thermal convection loops.

2. Methods

2.1 Experimental Setup

The acrylic loop used in this study was constructed to simulate bubble formation in the Molten Salt Thermal Convection Loop (MSTCL) operated at Soonchunhyang University. The overall configuration of the loop is shown in Figure 1. The loop consists of three acrylic pipe sections, a water reservoir tank, a circulation pump, and a flow meter. The first section is a vertical pipe through which water descends by gravity. The second section lifts the water upward using a pump. In the third section, the water rises and returns to the reservoir tank, completing the closed circulation. This arrangement enables continuous water circulation within the loop.

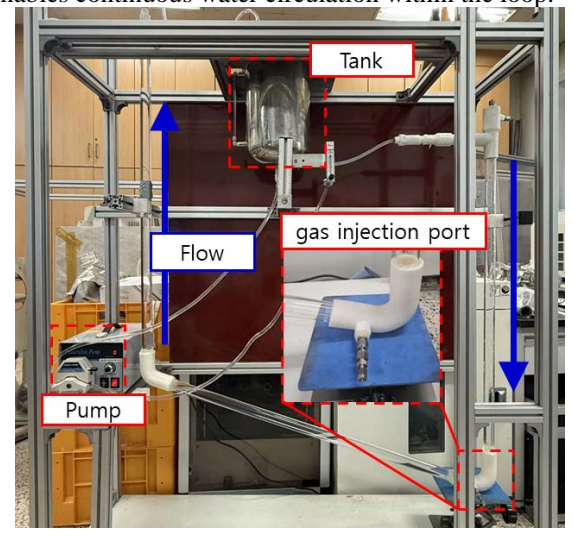


Fig. 1. Experimental setup of the acrylic circulation loop

To reproduce the geometry of the MSTCL, an argon gas injection port was installed at the lower end of the vertical section, where the loop transitions into the upward inclined segment. At this location, both buoyancy and bulk flow act simultaneously, allowing bubble behavior to resemble actual loop conditions.

Therefore, this point was selected as the analysis section. The inclined segment was designed with an angle of approximately 20°, consistent with the MSTCL configuration.

An argon gas injection nozzle was installed in the inclined section of the loop. The nozzle was fabricated from a 1/8-inch stainless steel tube, sealed at the tip, and drilled with eight outlet holes of 0.5 mm diameter. The holes were arranged in two rows, each containing four holes spaced 3 mm apart, with a vertical spacing of 1 mm between the rows. The nozzle was aligned with the bulk flow direction of the loop. Injected argon formed bubbles that were transported along the circulating stream. The loop was filled with water and circulated at a flow rate of 1.3 L/min using a pump. During circulation, argon gas was introduced through the nozzle at a pressure of 2 bar and a flow rate of 0.4 L/min, generating bubbles within the loop.

Under these conditions, the measured bubble velocity is interpreted as the apparent velocity that combines the bulk flow and the buoyancy-driven slip velocity, and it is distinguished from the terminal velocity of a freely rising bubble in stagnant fluids. Using the measured bubble size and velocity together with the known properties of water ($\rho=998~kg/m^3,~\mu=1.0\times10^{-3}~Pa\cdot s,~\sigma=0.072~N/m$ at $20~^{\circ}C$), key dimensionless numbers such as the Eötvös, Morton, and Reynolds numbers were calculated.

2.2 Bubble Imaging and Analysis

Bubbles formed inside the loop were recorded from a fixed observation point using video imaging at a frame rate of 30 fps. The acquired videos were processed using ImageJ software to quantify bubble size and rising velocity. It should be noted that the measured velocity under circulation conditions corresponds to an apparent velocity that includes both bulk flow and slip velocity components, whereas the Clift model provides predictions of terminal velocities in stagnant fluids. For comparison, the Clift correlation for pure systems was applied in this study, as shown in Equation (1) [4].

$$\begin{split} v_T &= 0.138 g^{0.82} \left(\frac{\rho_l}{\mu_l}\right)^{0.639} D_{eq}^{1.459}, \ D_{eq} < 1.3mm \ (1) \\ v_T &= \sqrt{\frac{2.14\sigma_l}{\rho_l D_{eq}} + 0.505 g D_{eq}}, \qquad D_{eq} \geq 1.3mm \end{split}$$

where v_T is the bubble rising velocity (m/s), g is the gravitational acceleration, ρ_l is the liquid density, μ_l is the liquid viscosity, D_{eq} is the equivalent bubble diameter (m), and σ_l is the liquid surface tension. The fluid properties for water at 20 °C were applied in this calculation, as described in Section 2.1.

3. Result

3.1 Bubble size and rising velocity

An example of the acquired images is presented in Figure 2. The bubbles were observed to adhere to the

upper wall of the acrylic pipe and move along the bulk flow direction. Most bubbles exhibited a spherical-cap shape attached to the ceiling. Based on these observations, the overall phenomena of bubble generation and motion are schematically illustrated in Figure 3.

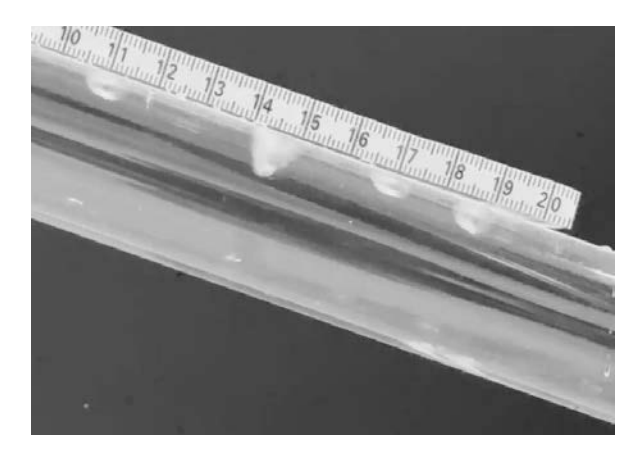


Fig. 2. Example image of bubbles observed in the loop

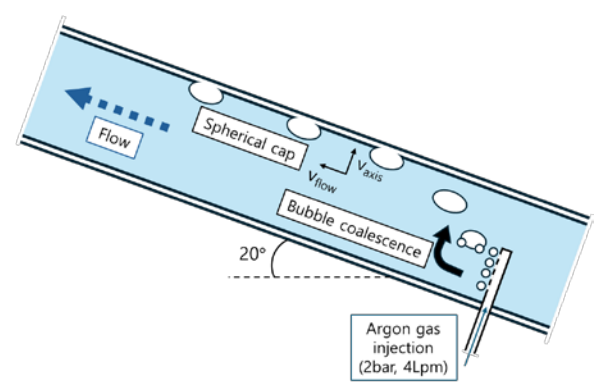


Fig. 3. Schematic illustration of bubble generation and motion in the acrylic loop

A total of 30 bubble trajectories were tracked through image analysis. Scale calibration was performed using both the ruler placed in the background and the known inner diameter of the acrylic pipe. Bubble volume (V) and equivalent diameter (D_{eq}) were calculated by assuming a spherical-cap geometry, as expressed in Equation (2).

$$V = \frac{1}{6}\pi h(3a^2 + h^2)$$
, $D_{eq} = \left(\frac{6V}{\pi}\right)^{1/3}$ (2)

where V is the bubble volume, a is the base radius of the spherical cap, and h is the cap height.

The rising velocity of each bubble was obtained from the centroid displacement over time along the inclined direction, as shown in Equation (3).

$$v_T = \frac{y_{i+1} - y_i}{0.033} \tag{3}$$

where v_T is the rising velocity of the bubble (mm/s), $y_{i+1} - y_i$ is the bubble displacement along the inclined direction between two consecutive image frames, 0.033 s is the time interval between frames (30 fps). The index i denotes the image frame number.

Bubbles with relatively large sizes in the range of 5-9 mm were observed. For quantitative evaluation, the bubbles were classified into four groups (5, 6, 7, and 8 mm), and the mean equivalent diameter, volume, rising velocity, and representative dimensionless numbers (Weber, Archimedes, Reynolds, Eötvös, and Morton numbers) were calculated. The definitions of these dimensionless numbers are given in Equation (4-8).

$$Eo = \frac{g\Delta\rho Deq^2}{2} \tag{4}$$

$$Eo = \frac{\sigma}{\sigma}$$

$$Mo = \frac{g\mu^4\Delta\rho}{\rho^2\sigma^3}$$

$$We = \frac{\rho v^2 Deq}{\sigma}$$

$$Ar = \frac{g\Delta\rho Deq^3}{\mu^2}$$

$$Re = \frac{\rho vD}{\mu}$$
(8)

$$We = \frac{\rho v^2 Deq}{\sigma} \tag{6}$$

$$Ar = \frac{g\Delta\rho Deq^3}{u^2} \tag{7}$$

$$Re = \frac{\rho v \dot{D}}{\mu} \tag{8}$$

where D_{eq} is the equivalent bubble diameter, v is the rising velocity, ρ is the liquid density, $\Delta \rho$ is the density difference, μ is the liquid viscosity, and σ is the surface tension.

The summarized results are presented in Table I. All values represent group-averaged results. The Morton number is identical for all groups 2.65×10^{-11} because it depends solely on the fluid properties (density, viscosity, and surface tension).

Table I: Bubble properties and dimensionless numbers by equivalent diameter group (mean values)

| ent diameter group (mean values) | | | | |
|----------------------------------|----------|--------|--|--|
| D_{eq} | V | v_T | | |
| (mm) | (mm^3) | (mm/s) | | |
| 5.6 | 92.58 | 226.23 | | |
| 6.44 | 140.05 | 229.16 | | |
| 7.44 | 216.01 | 235.68 | | |
| 8.21 | 290.05 | 244.1 | | |

| D _{eq} (mm) | Eo (-) | We (-) | Ar (-) | Re (-) |
|----------------------|--------|--------|----------------------|--------|
| 5.6 | 4.26 | 3.97 | 1.72×10^{3} | 1264.4 |
| 6.44 | 5.64 | 4.69 | 2.61×10^{3} | 1472.8 |
| 7.44 | 7.53 | 5.73 | 4.03×10^{3} | 1750 |
| 8.21 | 9.17 | 6.78 | 5.42×10^3 | 2000.1 |

3.2 Clift model calibration

The experimental results differed from those obtained under free-rising or vertical-rising conditions. In this study, the Clift (pure) correlation was applied to predict bubble rising velocity as a function of diameter and compared with the experimental data. As reported in previous studies [3], discrepancies become more pronounced for bubbles in the larger diameter range (≥ 1.3 mm), indicating that the model can be recalibrated to improve its accuracy. In this work, the correlation for $D_{eq} \ge 1.3$ mm was recalibrated by fitting the experimental data trend, and the modified equation is presented in Eq.

$$v_T = \sqrt{\frac{1.769\sigma_l}{\rho_l D_{eq}} + 0.509gD_{eq}} \tag{9}$$

Figure 4 presents a comparison between the experimental results and the model predictions. The symbols represent the mean rising velocity of 30 measured bubbles, grouped into diameter ranges of 5–8 mm, with error bars indicating the 25-75% interval. The calibrated correlation was compared with the original Clift (pure) model. Both results exhibited the same general trend of increasing rising velocity with bubble diameter in the 5-9 mm range. However, the experimental velocities were consistently lower than those predicted by the Clift correlation, which can be attributed to the wall-constrained motion of bubbles sliding along the ceiling of the acrylic pipe.

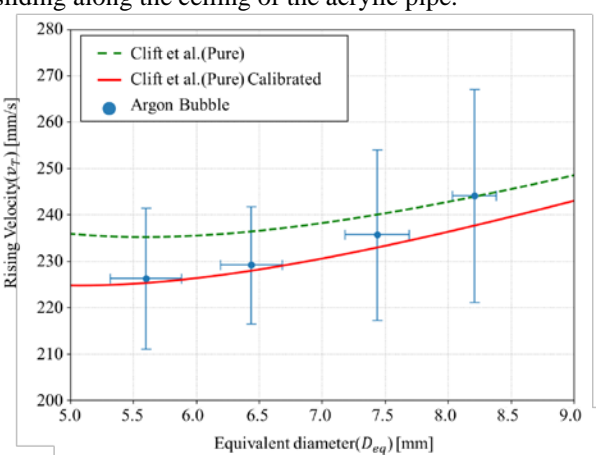


Fig. 4. Comparison of rising velocity between experimental data, the Clift (pure) model, and the calibrated model.

4. Conclusion

In this study, bubble dynamics in an acrylic water loop were experimentally investigated to simulate conditions relevant to the molten salt natural circulation loop. Bubble morphology and rising velocity were quantified through image analysis, and relatively large bubbles in the range of 5–9 mm were observed. The analysis also enabled the derivation of dimensionless numbers including the Eötvös, Morton, Weber, Archimedes, and Reynolds numbers, establishing a water-based surrogate dataset that provides a practical basis for scaling toward molten salt conditions.

The measured rising velocities were consistently lower than those predicted by the Clift (pure) model,

primarily due to wall-constrained motion along the pipe ceiling under circulation. Since the Clift correlation was originally developed for freely rising bubbles in stagnant fluids, its direct application under circulating flow is inherently limited. To address this discrepancy, the correlation for $D_{eq} \ge 1.3$ mm was recalibrated based on the observed data, resulting in improved agreement while retaining the general trend of increasing velocity with diameter.

These findings demonstrate the potential of applying calibrated correlations to predict bubble behavior under loop-specific conditions. Moreover, the water-based results provide a surrogate database that can be systematically extended to molten salt experiments through dimensionless scaling. Future work will focus on incorporating molten salt thermophysical properties, analyzing cover gas behavior, and validating the calibrated correlations under realistic molten salt natural circulation loop conditions.

Acknowledgement

This work was supported by the Korea Institute of Energy Technology Evaluation and Planning(KETEP) and the Ministry of Trade, Industry & Energy(MOTIE) of the Republic of Korea(No. RS-2023-00247323), This work was supported by the National Research Foundation of Korea (NRF) grant funded by the Korea government (MSIT) (RS-2023-00261146).

References

- [1] T. J. Dolan, *Molten Salt Reactors and Thorium Energy*, Woodhead Publishing, 2017.
- [2] J. Reis, J. Seo, and Y. Hassan, "Flow visualization experiments of argon injection in a molten salt natural circulation loop," *Physics of Fluids*, Vol.36, 043310, 2024. https://doi.org/10.1063/5.0205177
- [3] D. Orea, K. Robb, and J. McFarlane, "Comparative study between experimental measurements and model predictions of bubble rise velocity in molten LiCl-KCl," *Nuclear Engineering and Design*, Vol.443, 114247, 2025. https://doi.org/10.1016/j.nucengdes.2025.114247
- [4] R. Clift, J. Grace, and M. Weber, *Bubbles, Drops, and Particles*, Academic Press, 1978.